# UC Irvine
## UC Irvine Previously Published Works

**Title**

Modeling and comparison to literature data of composite solid oxide fuel cell electrode-electrolyte interface conductivity

**Permalink**

https://escholarship.org/uc/item/74w7w9c6

**Journal**

Journal of Power Sources, 195(21)

**ISSN**

0378-7753

**Authors**

Martinez, AS
Brouwer, J

**Publication Date**

2010-11-01

**DOI**

10.1016/j.jpowsour.2010.05.063

**Copyright Information**

Peer reviewed

# Modeling and comparison to literature data of composite solid oxide fuel cell electrode–electrolyte interface conductivity

Andrew S. Martinez, Jacob Brouwer*

National Fuel Cell Research Center, University of California, ELF 221, Irvine, CA 92697-3550, United States

## ABSTRACT

A Monte Carlo percolation model previously used to characterize Triple Phase Boundary (TPB) formation in composite SOFC electrode–electrolyte interfaces has been augmented to allow for investigation of the effects of composition, gas-phase percolation, and surface exchange and transport phenomena on the overall conductivity of these electrode–electrolyte interfaces. The model has been utilized to replicate the results of a previous modeling effort, with similar assumptions and application to an SOFC electrode electrolyte interface. Although the models are similar in many aspects, their key differences allow equivalent predictions of the behavior of overall electrode conductivity as a function of electrode composition, thereby verifying the assumptions and overall approach of the current model. The validity of omitting charge-transfer and activation resistances when comparing overall interfacial conductivity trends is confirmed. The current model is then used to simulate several experimental results. The comparisons among these results show the importance of including gas-phase percolation physics and surface exchange and transport phenomena features in the model. Including gas-phase percolation and these surface phenomena can significantly alter the predictions of conductivity behavior and better predicts experimental observations, particularly at low and high electronic conductor volume fractions.

© 2010 Elsevier B.V. All rights reserved.

## 1. Introduction

The development of any successful solid oxide fuel cell (SOFC) microstructure model is inherently dependent upon proper understanding of the techniques and processes utilized in SOFC manufacturing. The common techniques for preparation of the materials used to form an electrode include ceramic materials synthesis, particle manufacturing and sizing, randomized mixing of particles, addition of binders, surfactants, and pore-forming agents, ball milling, and sintering. Many different processing steps can then manufacture these materials into the desired electrode and electrolyte structures and form functional electrode–electrolyte interfaces. These processes include screen printing, tape casting, tape calendaring, magnetron sputtering, flame and plasma spraying, and aerosol-assisted vapor deposition [1–8]. Through these processes, the various material phases that comprise the electrode structure and the electrode–electrolyte interface are typically organized according to random mixing processes. While generally effective, these random particle placement processes lack spatial or property correlation or control and are not amenable to detailed engineering of the interfacial microstructure. These random processes apply to both the solid phase and the pore microstructure of the final electrode construction since pore development is governed by the inclusion and random placement of pore-forming particles in the manufacturing of the electrode–electrolyte interface.

The effects of these processes and the various features of the raw materials on fuel cell performance have been investigated through many previous studies by empirical methods and the development and application of models [9–14]. Experimentalists have identified many parameters that are important to manufacturing electrode–electrolyte interfaces with low ohmic and/or activation losses. For example, researchers such as Sasaki et al. have identified that material properties such as particle size distribution are particularly important [9–11]. In addition, Sasaki et al. and Juhl et al. have found significant dependence upon manufacturing parameters such as electrode thickness [9,12] and processing temperatures including calcining and sintering steps [9,10,13]. Dusastre and Kilner have demonstrated the benefits of including multipurpose materials such as mixed electronic–ionic conductors (MEIC) [13]. A recent visualization study by Wilson et al. [14] has begun to provide mechanistic insights through investigation of the electrode microstructural and compositional parameters such as tortuosity, interfacial adhesion, and interconnectivity in an effort to provide greater insight and improved detail with regard to these factors and how they affect percolation in the electrode.

* Corresponding author. Tel.: +1 949 824 1999x221; fax: +1 949 824 7423.
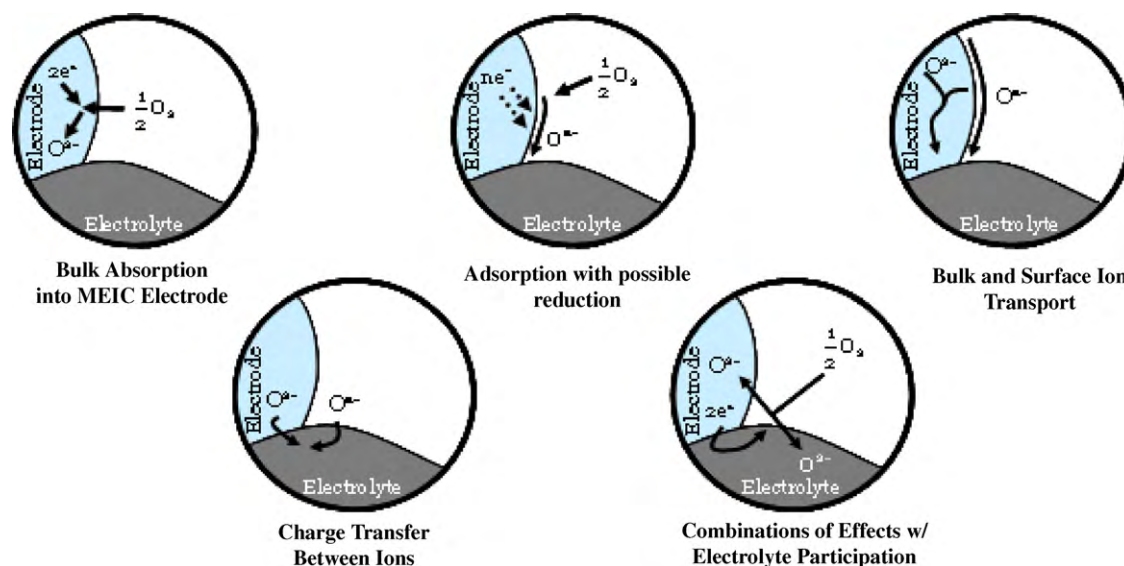   *E-mail address:* jb@nfcrc.uci.edu (J. Brouwer).

**Fig. 1.** Reaction mechanisms involved in surface exchange and transport phenomena at an SOFC cathode [22].

Moreover, the modeling investigations carried out thus far have confirmed experimentally observed relationships and provided mechanistic insight into these relationships. Models have also contributed novel observations about electrode performance and its relationship to interfacial microstructure. In particular, the dependence of performance on the physical size of particles and the entire electrode have been recreated through simulation by researchers such as Costamagna et al., Deseure et al. and others [15–19]; the dependence on electrode composition has been repeatedly found to be of particular importance [15–17,19–21]; the dependence of likelihood of TPB formation on location within the electrode has been characterized by the work of Costamagna et al. as well as through the current model [21,15]; the dependence on the ratio of electronic-to-ionic conductivity has been identified [16]; the effect of functional and compositional grading in the electrode has been characterized by Deseure et al. and Schneider et al. [17,19]; the dependence of TPB formation on the geometry of the current collector and the intermixing of gaseous and electronically conducting phases in this boundary has been noted to be of particular importance through the previous use of the current model [21]; and the approximation that a TPB length is roughly three times the radius of a representative particle has been calculated [20].

The current work is built upon a previously developed two-dimensional Monte Carlo model that was used to investigate some of these phenomena [21]. The model differs from those presented above in that it includes novel consideration of the gas phase as a percolating network with just as much impact on performance as the percolation of the ionic and electronic phases. The current work augments the model to simulate conductive performance measurements by development and application of a method to calculate the conductivity of an arbitrary, randomly organized conductivity network. The previous work with this model [21] has supported the understanding that the high energy conversion efficiency often attributed to fuel cell operation is critically dependent upon the morphology of the microstructure of the fuel cell electrode–electrolyte interface. It was particularly demonstrated that in this interfacial region, and within the structure of the electrode itself for composite electrodes, the necessary phases (gas, ionic conductor, and electronic conductor) form intertwining pathways and structures, with TPBs forming at the locations where these pathways all come into contact. In particular, the percolation of the gas phase through the electrode has been investigated

and shown to have a marked impact on the formation of active TPBs in the electrode. The effects of the gas phase physically extend beyond the gaseous pathways in the electrodes themselves, as the gaseous reactant and product phases are subject to surface exchange and transport phenomena, as discussed in [22] and modeled in [21], and shown in Fig. 1. The formation of these TPBs serves as the basis for enabling chemical reaction and therefore increasing the potential for high efficiency of the entire fuel cell. However, these surface exchange and transport phenomena can also have a marked effect on the conductivity of the electrodes in which the TPBs form. Not only is the number of TPBs formed important, but also location within the electrode, interconnectivity, and the length of conducting paths leading to and from each TPB are also important. The formation and location of TPBs, including their dependence upon interconnectivity of phases and interaction with the current collector geometry, have previously been investigated [21]; these observations can now be extended to the overall conductance (akin to the inverse of area specific resistance, ASR) of the electrode–electrolyte interface.

## 2. Model description

The calculation of the overall conductivity for a given simulated electrode is directly dependent on the number and location of TPBs formed within its structure; thus, the full functionality of the previous model was utilized in this investigation, with the addition of the conductivity calculation. The model has been used previously [21] to investigate various parameters of the construction and structure of composite fuel cell electrodes. In particular, porosity, volume fraction of electronic and ionic conducting materials, the addition of mixed conducting materials, surface exchange and transport phenomena, and current collector geometry have been previously investigated and characterized [21]. The model was also developed to allow investigations of the effects of particle size distributions in the different solid material phases as well as the pores [23]. Some characteristics that are pertinent to percolation physics and microstructure characterization, such as tortuosity, are not explicitly defined or evaluated in the model. However, the simulated interfaces generated by the model did recreate these features in their two-dimensional rendering. This is clear from observation of the twisting paths shown in Fig. 2 as well as the model development described in [21]. The model in this work is a direct extension
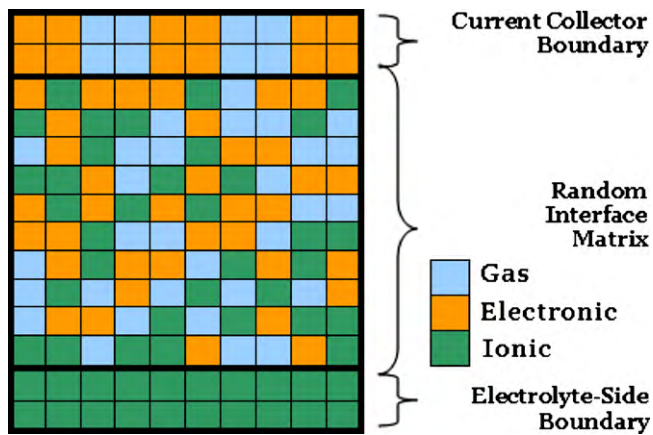
**Fig. 2.** Sample randomized monodispersed interface structure: blue denotes gas, orange denotes electron conducting phase, and green denotes ion conducting phase. (For interpretation of the references to color in this figure legend, the reader is referred to the web version of the article.)

of the previous model and therefore included all of the capabilities described in the previous work [21,23]; additionally, the model in this work includes a process for analyzing the resulting conductivity network within the electrode–electrolyte interface and calculating the effective conductivity of this network.

Briefly, the previous model was characterized by the formation of randomized square matrices consisting of prescribed amounts of various phases of material. The electron conducting, ion conducting and gas phases are the pertinent phases in this investigation. Given that all three of these phases are considered to be equal in both this and the previous work, the model has been formulated to require the same percolation characteristics from the gas phase as are required of the solid electron and ion conducting phases [21]. Boundary conditions were established to model a dense electrolyte on one side of the electrode structure, and an assumed geometry for the current collector on the opposite side, consisting of only gaseous and electronic conductor phases. A sample of the model geometry and structure is presented in Fig. 2. Through an iterative process of path and adjacency identification, the total number of TPBs was obtained for each Monte Carlo iteration. Sufficient random seeds and iterations (10,000) were used to gather statistically significant results for various electrode compositions that were compared to each other. In the previous investigation, potential TPBs and active TPBs were considered; however, for the current work, only those "active" TPBs, which are defined by adjacency of all three necessary phases in addition to the formation of continuous paths to the appropriate bulk phase, are considered. As previously stated, this requirement is applied equally to the gas phase and the solid phases. Thus, when surface exchange and transport phenomena is not enabled, TPBs are only considered to be formed at the corners of the simulation lattice where all three particle phases are present with the required connections to supporting bulk phases. This should not be taken to imply that the TPBs are themselves envisioned to occur at a single point; the use of counting the TPBs at the points is merely the two-dimensional analog of the TPB line that would be present in a three-dimensional structure. However, with surface exchange and transport phenomena enabled, the effective TPB length is extended to the total active TPB area that is actually present in electrode–electrolyte interfaces. Surface exchange and transport phenomena, which is comprised of many physical absorption and transport processes in the vicinity of the TPB [22], was approximated in the current model by considering gas particles that percolated to a location one cell removed from an electronic–ionic conducting material interface to count as completing the formation of the TPB at that point. This

was the only aspect in which the gas phase was treated differently.

The use of a two-dimensional model in this work deserves some clarification. Although the current study clearly relies on percolation physics, there are many factors that set it apart from the traditional percolation analysis. Primary among these differences is the inclusion of multiple percolating phases. The percolation of one phase is well-understood in classical percolation theory, but the problem of multiple percolating phases has yet to be fully characterized. To-date, the only known geometry for which two phases can percolate simultaneously is bond percolation on a triangular lattice [24]. Normally, one must also therefore consider the percolation threshold for the problem. For a given lattice geometry and percolation type, the percolation threshold describes, for a single-phase percolation problem, the minimum volumetric fraction of the particle required for a percolating cluster to form within one random dispersion of particles within an infinite domain. It should also be noted that the number of dimensions considered has a significant effect on this measure, usually resulting in a lower percolation threshold with increasing number of dimensions, indicating a higher probability of forming a percolating cluster when particles are randomly arranged in the lattice. However, percolation thresholds are not yet well-characterized for the multi-phase problems, in either two or three dimensions. In addition, use of a two-dimensional model allows study of a much greater and statistically significant number of instances in the Monte Carlo simulation as well as consideration of various boundary conditions and multi-phase percolation to designated bulk phases, which has not previously been analyzed.

Thus, the current investigation adopts a new percolation framework, based upon modifications to traditional percolation analyses, which is established to better match the physics and behavior of a fuel cell interface. In this study, percolation was considered to occur not only along particle edges but also at corners. This assumption accounts for the high-temperature manufacturing process of sintering that induces the formation of necks between adjacent particles, thereby connecting those particles that may not have been touching in the original, unprocessed geometry. Therefore, inclusion of percolation through corners accounts for this physics, producing a more realistic definition of a percolating cluster than the conventional method. In addition, unlike the traditional percolation problem, this investigation explores a statistically significant set of finite domains (Monte Carlo method), thereby not seeking a theoretical optimum, but one more directly applicable to real interfaces. Moreover, the phases that must be connected within the geometry being considered do not need to span the entire length of the geometry in order to generate a TPB. Instead, the phases must percolate from different sides and meet at some point(s) in the body of the geometry in order to from a TPB; thus, the percolation need not be as extensive as that required for a conventional percolation study, and the percolation threshold should have less of an impact. Finally, due to the non-uniform geometry of real current collectors, the connection of a percolating electronic or gas cluster to this edge is not as simple nor is it guaranteed as in typical studies. This can thereby limit the ability to form active, percolating clusters of these phases in the interface.

Thus, certain aspects of the current model are less rigorous than that required by the classic percolation problem while others are more rigorous in addressing electrode–electrolyte interface physics. In addition, the definition of the current problem is more complex and requires consideration of more variables than one simple set of volume fractions and/or coordination numbers. With all of these modifications, the classical definition of the percolation threshold does not address the unique features of the fuel cell interface problem under consideration. This work analyzes the effects of percolation physics within this revised framework by considering:
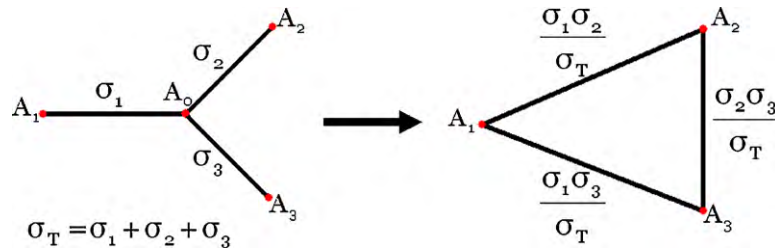
**Fig. 3.** Sample node elimination by method of Fogelholm [26–28].

(1) corner percolation accounting for necking during manufacture, (2) percolation of three phases, (3) statistically significant representations of interface geometry, and (4) edge and design effects of the interconnects.

It should also be noted that although the particle size and shape distribution may have an effect on the morphology of the interface and the percolation physics, the simulation results collected for this work were all for a monodisperse case; all particles were assumed to be the same size of one simulation cell. It is unclear from previous work whether or not the particle size and shape distributions are significant factors of percolation physics that affect overall cell performance [9–11,23].

Once the TPBs are identified by the model, the conductivity can be calculated, first on a per-TPB basis, and then for the overall simulated electrode–electrolyte interface. Algorithms have previously been developed for this problem [25–29]. However, as noted by Gingold and Lobb [29], the method described by Fogelholm [26–28] is an efficient and easily implemented algorithm. The basis of the algorithm is the replacement of any conducting node that has any number of conducting pathways between it and other conducting nodes with pathways between the other conducting nodes that produce an overall equivalent conductance. The method thus relies on a single definition for a node transformation, as opposed to the multiple definitions required by the approach of Frank and Lobb [25]. In addition, Gingold and Lobb have shown that the single node transformation method can be successfully applied to models that were not under consideration in the original formulation of Fogelholm's method, including an extension to higher dimensions than that used in the original model formulation. Thus, this investigation relies on this simple node transformation algorithm for the basis of its conductivity calculations.

The formulation of the node elimination step follows the form:

- If node $A_0$ is connected to nodes $A_1, A_2 \ldots A_n$, by conducting paths $\sigma_1, \sigma_2 \ldots \sigma_n$.
- Remove the node $A_0$ along with conductances $\sigma_1, \sigma_2 \ldots \sigma_n$.

Insert conductances $\sigma_{ij} = \dfrac{\sigma_i \sigma_j}{\sum_1^n \sigma_k}$ between every pair of nodes

$$A_i \text{ and } A_j. \tag{1}$$

A sample of this calculation is shown in Fig. 3 for the simple case of a common Y-$\Delta$ transformation. Any connections that become parallel conducting paths or terminations to dangling nodes as a result of this process can then be simplified at the conclusion of each iteration of the algorithm. Iterative application of this algorithm to an arbitrary network results in a single conductor connecting the endpoints of the network with a conductance value equivalent to that of the entire original, randomized network.

In order to make use of this algorithm, the data that defines each instance of a randomized network in the Monte Carlo model had to be converted to a form applicable to these calculations.

Both electrically and ionically conducting paths were defined by the edges of the particles that formed the interconnected paths of each particle phase. This allows for ready inclusion of conduction through corners of particles, which accounts for the physics associated with necking between particles during normal manufacturing processes in fuel cell electrodes. Although conduction paths were identified as associated with particle surfaces, surface conduction was not assumed. Rather, the surfaces were merely used as references to allow for the possible formation of multiple conduction paths between particles (which may occur in particles with necked geometries), with the physics of conduction modeled as through the bulk of the materials. In fact, the bulk conductivities for all materials and particle cross-sectional areas were utilized to calculate overall conductance in this investigation.

A sample of the identification of these conducting paths is provided in Fig. 4. The location at the center of the blue box represents an active TPB, for which the electronic conductivity was calculated as the conductivity between the TPB and the terminal X, and the ionic conductivity calculated between the TPB and terminal Y. The reduction algorithm therefore operated separately on the electronically and ionically conducting paths and then the two conductances were combined in series, with all TPBs assumed to act in parallel. Thus, the overall conductivity of any particular electrode–electrolyte interface was calculated as:

$$\sigma_{\text{electrode}} = \sum \sigma_{\text{TPB}}, \quad \text{where } \sigma_{\text{TPB}} = \frac{\sigma_{\text{ionic}} \sigma_{\text{electronic}}}{\sigma_{\text{ionic}} + \sigma_{\text{electronic}}}. \tag{2}$$

For all investigations, both the overall conductivity and the conductivity per TPB were calculated. However, it should be noted that the conductivity per TPB simulation results did not include any results from interface structures that developed no (zero) TPBs; therefore, in select cases, the conductivity per TPB appears higher
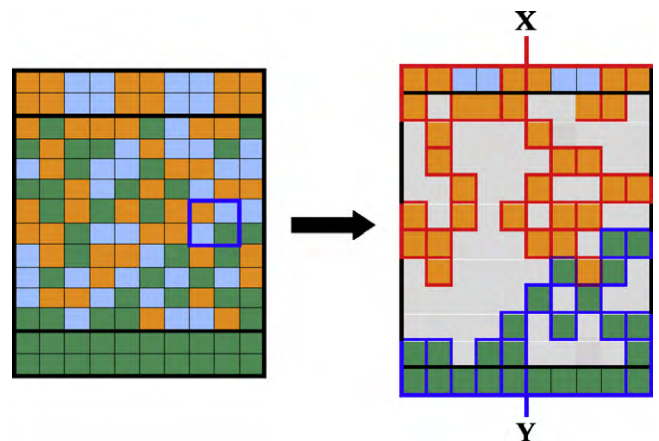


**Fig. 4.** Sample conversion of randomized electrode matrix to conducting paths: red denotes pathways of electronic conductance, blue denotes pathways of ionic conductance, and purple denotes pathways available to both conductances. (For interpretation of the references to color in this figure legend, the reader is referred to the web version of the article.)

than the total conductivity only because the average number of TPBs per electrode (which does include cases when no TPBs are formed) is less than one. It should also be noted that the boundary particles were assumed to be infinitely conductive so that the boundary structure and material properties (e.g., interconnect, bulk electrolyte material) did not affect the calculations. Due to this assumption, adjustments for TPBs lying on particles adjacent to either boundary were included in the definition of the electronic and ionic conductivities so that the calculated conductivity would not be infinite; instead, the conductivity through the interface in these cases would be completely defined by the conducting path of the particle type not matching the boundary on which the TPB lies.

Although the effect of surface exchange and transport phenomena serves to increase the proportion of the electrode that is electrochemically active, it also carries with it additional losses related to the physical, chemical and electrochemical processes involved. Following the processes outlined by Adler [22], the current model includes three major surface exchange and transport phenomena processes that can affect electrode overpotential: (1) adsorption of ions into the solid material phases of the electrode, (2) adsorption of electrons into the charge double layer and the solid phases of the electrode, and (3) migration of oxygen vacancies in the ion conducting phase of the electrode. Although these three mechanisms do not comprehensively address the reaction and transport physics thought to occur near the TPB, they represent the major processes and are sufficient to investigate how these mechanisms can alter cell overpotential. The overall method for including these physics in the current model is to add a conducting element, in series with the remaining electrical network, at TPBs in the conducting network only when the TPB was formed by the action of surface exchange and transport phenomena. Thus, even in simulations with surface exchange and transport phenomena physics enabled, the additional element was only included for those TPBs at which all three phases where not in physical contact.

The calculation of the conductance associated with surface exchange and transport phenomena was formulated by assuming an electrode overpotential, calculating the current attributable to these processes, and following Ohm's law to arrive at an overall conductance representative of the action of surface exchange and transport phenomena. Thus, the overall rate of the processes was related to the current by:

$$r_{\text{ads,ion}} + r_{\text{ads,elec}} + r_{\text{vacancy}} = \frac{i}{nF} \tag{3}$$

where the terms on the left represent the rates of adsorption of oxygen ion species, adsorption of electrons, and migration of oxygen vacancies, respectively. The rates of reaction were defined as follows [17]:

$$r_{\text{ads,ion}} = V a_{\text{v,ads}} \Gamma^2 k_{\text{ads}} P_{O_2} (1 - \theta)^2 \tag{4}$$

where $a_{\text{v,ads}}$ is the volume-specific surface area available for adsorption. The volume-specific surface area available for adsorption is defined by [17]

$$a_{\text{v,ads}} = \frac{N_P \pi d_p \tau L}{V}, \tag{5}$$

$$r_{\text{ads,elec}} = V a_{\text{v,TPB}} \Gamma k_e \, \exp\left(\frac{-2\alpha F}{RT}\eta\right) \theta c_v^{\text{YSZ}} \tag{6}$$

where $a_{\text{v,TPB}}$ is the volume-specific TPB surface area. Volume-specific TPB surface area is estimated according to [17] as

$$a_{\text{v,TPB}} = a_{\text{v,TPB,0}} \left(1 - \frac{\varepsilon - \varepsilon_{\text{FCC}}}{1 - \varepsilon_{\text{FCC}}}\right) \frac{d_{p,0}^3}{d_p^3}, \tag{7}$$

$$r_{\text{vacancy}} = d_p u_v c_v^{\text{YSZ}} \nabla E \tag{8}$$

**Table 1**
Summary of physical constants in surface exchange and transport phenomena model.

| Constant | Description | Value | Reference |
|---|---|---|---|
| $V$ | Electrode volume | $2 \times 10^{-9}\,\text{m}^3$ | Current |
| $\Gamma$ | Adsorption sites per unit area | $10^{-5}\,\text{mol m}^{-2}$ | [17] |
| $k_{\text{ads}}$ | Adsorption rate constant | $10^4\,\text{m}^2\,(\text{mol atm s})^{-1}$ | [17] |
| $P_{O_2}$ | Oxygen partial pressure | 0.2 atm | [17] |
| $\theta$ | Surface coverage | $10^{-4}$ | [17] |
| $N_p$ | Number of pores | $1.5 \times 10^{-5}$ | Current |
| $d_p$ | Particle diameter | $2\,\mu\text{m}$ | Current |
| $\tau$ | Tortuosity | 1.6 | [17] |
| $L$ | Electrode thickness | $20\,\mu\text{m}$ | Current |
| $k_e$ | Electron transfer rate constant | $10^4$ | [17] |
| $\alpha$ | Symmetry factor | 0.5 | [17] |
| $F$ | Faraday's constant | $96{,}485\,\text{C mol}^{-1}$ | N/A |
| $R$ | Gas constant | $8.314\,\text{J}\,(\text{mol K})^{-1}$ | N/A |
| $T$ | Operating temperature | 1000 K | Current |
| $\eta$ | Electrode overpotential | 30 mV | Current |
| $C_v^{\text{YSZ}}$ | Vacancy concentration in YSZ | $6000\,\text{mol m}^{-3}$ | [17] |
| $\varepsilon$ | Porosity | 0.3 | Current |
| $\varepsilon_{\text{FCC}}$ | Theoretical porosity of FCC lattice | 0.26 | [17] |
| $d_{p,0}$ | Reference particle diameter | $1\,\mu\text{m}$ | [17] |
| $q$ | Charge of ion | $3.204 \times 10^{-19}\,\text{C}$ | Current |
| $k_B$ | Boltzmann's constant | $1.381 \times 10^{-23}\,\text{J K}^{-1}$ | N/A |
| $D$ | Oxygen diffusion coefficient | $0.303 \times 10^{-10}\,\text{m}^2\,\text{s}^{-1}$ | [17] |

where $u_v$ is the oxygen ion mobility, defined as

$$u_v = \frac{q}{k_B T} D \tag{9}$$

The various physical constants used in the current surface exchange and transport phenomena model are defined and quantified in Table 1. Note that the number of pores was calculated assuming the overall electrode dimensions were 1 cm by 1 cm, and that 30 pores in a given simulated electrode were representative of the number of pores on a 2-$\mu$m slice of the electrode. With the values defined in Table 1, the three rates that contribute to surface exchange and transport phenomena were calculated as

$$\begin{aligned} r_{\text{ads,ion}} &= 6.33 \times 10^{-12}\,\text{mol s}^{-1} \\ r_{\text{ads,elec}} &= 1.00 \times 10^{-11}\,\text{mol s}^{-1} \\ r_{\text{vacancy}} &= 2.53 \times 10^{-13}\,\text{mol s}^{-1} \end{aligned} \tag{10}$$

The relative values of these three rates are worthy of discussion. First, the span of these rates is not very large, indicating that these three processes contribute roughly equally to overall surface exchange and transport phenomena (i.e., none can be neglected in comparison to the others). Second, the relative magnitudes of these rates places them in an order of swiftness that is consistent with intuition: adsorption of electrons is the fastest process, followed by adsorption of ions onto the solid phases, and finally followed by transport of ions through the solid electrolyte phase. From these rates, the total overall conductivity associated with surface exchange and transport phenomena was calculated according to

$$\begin{aligned} i_{\text{Sorbate}} &= 4F \cdot (r_{\text{ads,ion}} + r_{\text{ads,elec}} + r_{\text{vacancy}}), \\ S_{\text{Sorbate}} &= \left(\frac{\eta}{i_{\text{Sorbate}}}\right)^{-1} \\ \sigma_{\text{Sorbate}} &= \frac{S_{\text{Sorbate}}}{d_p} \end{aligned} \tag{11}$$

where it is assumed that 4 electrons are involved in the overall reduction of each mole of diatomic oxygen molecules. The overpotential presented in Table 1 is associated only with surface processes and as such is entirely attributed to the surface exchange and transport phenomena processes in the current model, and the surface exchange and transport phenomena conductivity is effective over one particle diameter's length, as mentioned above.

G/E G/E G/E G/E G/E G/E G/E G/E G/E G/E G/E G/E G/E G/E

**Fig. 5.** Idealized uniform current collector and gas delivery boundary condition.

Utilizing these rates, the overall surface exchange and transport phenomena conductance was found to be 2.14 S cm$^{-1}$. This conductance value has an order of magnitude significance that is sufficient to alter the overall conductance attributed to a TPB that is formed via surface exchange and transport phenomena by a substantial value. The overall effect on the entire electrode's conductivity, however, can only be determined by the full simulation utilizing this additional conductance, and is discussed below.

### 2.1. Model execution

Following the formulation of the previous investigation [21], simulation results for the conductivity of the electrodes were collected for cases with a 30% porosity, over a full range of mixtures from all-electronic to all-ionic, in increments of 5% increase in the ionic phase volume fraction. Data were collected for 10-by-10 particle randomized electrodes, with statistics gathered over 10,000 Monte Carlo iterations of the calculations. It should be noted that the number of particles in the simulated electrode and the number of iterations match the values used in the previous investigation of TPB formation. Fewer iterations would not have been desirable, given that it is expected that the conductivity results are related to active TPB formation, for which these simulation parameters were previously found to be necessary. The effect of surface exchange and transport phenomena has been investigated in the activation of electronic–ionic interfaces isolated from direct contact with the gas phase and found to significantly affect the amount of active TPBs found in the overall electrode–electrolyte interface [21]; thus, data have been collected for this investigation for cases with and without surface exchange and transport phenomena. Finally, the current collector boundary condition was modeled as the idealized situation shown in Fig. 5, where every particle in this boundary is able to conduct electrons and gas. Although this is not a physically realizable geometry, it was chosen to provide the least limiting case for overall interfacial conductivity and also to facilitate comparison with previous modeling efforts in the literature (which do not account for current collector geometry).

## 3. Results

### 3.1. Evaluation of surface exchange and transport phenomena surface conductivity

Although it is important to understand the many processes that take place in surface exchange and transport phenomena and to investigate how they affect overall conductivity, it is easily recognizable that the surface reaction conductivity associated with surface exchange and transport phenomena is similar in function to an activation resistance, at least in the context of the overall conducting network. A sensitivity analysis of surface exchange and transport phenomena was accomplished to determine whether or not it was necessary to include such physics in the model. This was done by running the model both with and without surface exchange and transport phenomena conductivity enabled at TPBs formed only by surface exchange and transport phenomena. The conductivity, conductivity per TPB, and normalized (to the maximum of the data set) conductivity and conductivity per TPB were calculated for all electrode compositions in both cases and compared through the use of Analysis of Variance (ANOVA).

The results of ANOVA for the normalized electrode conductivity are presented in Table 2. When the surface conductivity was taken to be the only factor influencing the overall electrode conductivity, it was found that this factor did not play a significant role in the final result. This is as indicated by the high $p$-value of 0.9869, which indicates that the difference between the data with and without the surface conductivity is not significantly different from what would be expected due to simple random variation in the data sets. Further evidence of the inconsequential contribution that surface exchange and transport phenomena conductance makes to overall interfacial conductivity is presented below, especially through comparisons with similar models that include a conductance with this same type of functionality. Additionally, although they are not shown, all four of the measures mentioned above provided the same conclusion; the dependence of the conductivity calculation was independent of whether or not the surface exchange and transport phenomena-related conductivity was included in the model. Note that accounting for surface exchange and transport phenomena is important for accurate simulation of electrode–electrolyte interfaces, but the resistance introduced by surface exchange and transport phenomena physics appears to be low in comparison to other contributions to overall interfacial resistance. Thus, the results presented in [21] that show surface exchange and transport phenomena to be significantly influential in the formation of TPBs still hold; it is simply the effect of the associated electrical resistance that is not significant.

### 3.2. Comparison to previous model in the literature

In order to validate the formulation of the conductivity model, the entire Monte Carlo simulation process was carried out with modifications that allowed a direct comparison to a previous work that was similar to the current investigation. Sunde [20] developed a model of a composite electrode, but did not include the effects of gaseous percolation; instead, gas was assumed to be present throughout the entirety of the electrode and therefore uninhibited by the structure of the solid phases. To approximate this condition, the current model was modified to simply impart perfect gas phase conductivity on all particles in the randomized portion of the electrode–electrolyte interface. Thus, the entire interface was constructed of electronically and ionically conducting particles that also carried the gas phase properties. This approximates solid particles with sufficiently interconnected micropores such that no path for transport of gaseous species is completely blocked and wherein no diffusion limitations exist. The previous work assumed an electrode where the electronically conducting phase was nickel, with a conductivity of 20,000 S cm$^{-1}$ and the ionically conducting phase was YSZ, with a conductivity of 0.1 S cm$^{-1}$ at an

**Table 2**
ANOVA analysis results for the sensitivity of calculated conductance to inclusion of surface exchange and transport phenomena-related surface conductance.

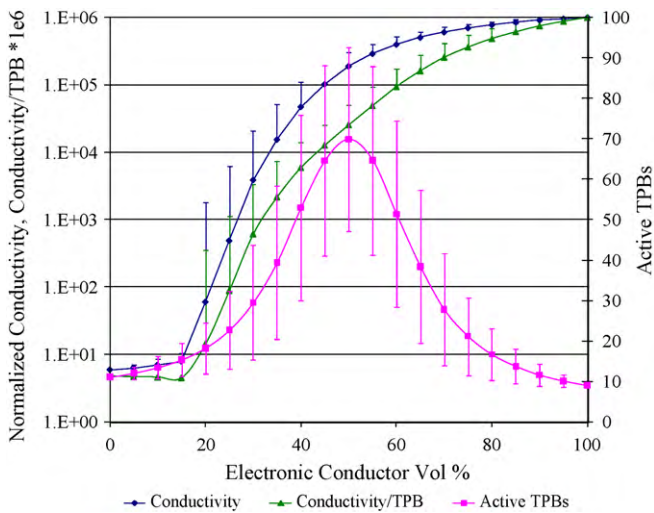| Response 1: normalized conductivity Transform: natural log | | | | | | Constant: 0 |
|---|---|---|---|---|---|---|
| Source | Sum of squares | df | Mean square | $F$-value | $p$-Value Prob > $F$ | |
| Model: surface conductivity | 0.004 | 1 | 0.004 | 0.000 | 0.9869 | Not significant |
| Residual | 426.822 | 28 | 15.244 | | | |
| Cor total | 426.826 | 29 | | | | |

**Fig. 6.** Active TPBs and calculated conductivity from replication of Sunde's assumptions with the current model.

operating temperature of 1000 °C. The ratio of these conductivities (electronic-to-ionic) is defined as the phase contrast, an important aspect in the overall conductivity of an interface.

The conductivity calculated for this reconstruction of the model without gas phase limitations is shown in Fig. 6. The data points in Fig. 6 represent the average values over 10,000 randomized simulations, with error bars representing one standard deviation; which is true of the similar figures that follow in this work. It should be noted that conductivity has been normalized to the conductivity value calculated at the peak conductivity, which occurred at the all-electronic composition. As previously discussed in similar models, the optimal composition for the electrode conductivity is very different from the compositions found by the model to be advantageous for TPB formation [21], which the current model determined to be 10% electronic conductor. The data of Fig. 6 is compared to that of Sunde's original work in Fig. 7 and found to be in overall good agreement with his previous findings.

There are certain differences between the results of these two models that deserve special consideration and discussion. The first major difference between the model results is the electrode composition at which the sudden rise in conductivity occurs. In the
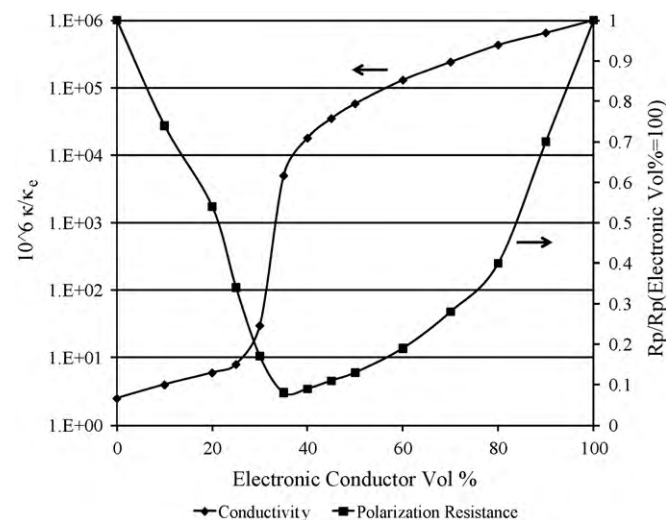
current investigation, the sudden rise occurs between 15 and 20% electronic volume fraction; whereas in the previous study, the rise occurs at a slightly higher 25–30% electronic volume fraction. This could be due to the particle placement algorithm of the two models, which are not identical. Particles in the current investigation are positioned along a pre-defined grid structure, whereas the particle placement in the prior model was according to a random-packing model. This can affect the percolative properties since the percolation limit in these two scenarios is not equivalent [24], which can alter the composition at which conductivity suddenly rises. In addition, the dependence of the conductivity upon composition (slope) in this rapidly increasing region is greater in the Sunde model. This may be related to the difference in the composition at the commencement of the rise, given the nature of the normalization scheme, which requires that both data sets reach the same maximum.

Although the two models are similar in key aspects of model setup and execution, there are still some differences between them which provide interesting insight, given the close match between the results of Figs. 6 and 7. The first of these is that the previous model, and many others in the literature, includes a charge-transfer conductance between electronic and ionic particles as well as an equivalent conductance to account for activation polarization in the calculation of their percolating path conductivities. The electronic-to-ionic conductivity in this model was defined as

$$\sigma_{ed-el} = [(2\sigma_{ed})^{-1} + (2\sigma_{el})^{-1} + \sigma_p^{-1}] \qquad (12)$$

where $\sigma_p$ is the conductivity associated with the activation polarization. Although inclusion of this conductivity certainly alters the absolute value for any given full electrode conductivity calculation, it can be seen that for the purposes of comparing conductivity of electrodes of varying compositions, this particular feature can be neglected. It can be considered that these conductivities, even if included in the calculation, will equivalently affect each individual conductivity calculation at every TPB, and therefore not be observable in a comparison of conductivities. They would effectively "drop out" of the calculation through comparison. This is explicitly ensured in the data as presented, since all data are internally normalized to the maximum value in the data set itself. This, however, is only true for cases when the electrode's potential varies linearly with the conductance presented in Eq. (12). This operating condition only occurs in cells where the dominant rate-determining step is the surface exchange process. For Ni–YSZ, a representative value for this conductance is $10^{-4}$ S cm$^{-1}$, which, compared to the conductances utilized in this model, may be able to establish this rate-determining condition [20].

It should also be noted that in addition to the difference in the placement of particles, conduction pathways are defined in different manners for the two models. As previously discussed, the existence of a conducting pathway is indicated by particle edges in this work; however, in the Sunde formulation, the conduction path is defined by particle bonds, according to a bond percolation scheme. Again, the close match between the model results from each of the two investigations serves as an indication that the formulation of the current model, though different from the previous work, is equally valid.

In addition, the active TPB counts of the current model without gas phase limitations can be directly compared to data reported previously in [21], for which gas-phase percolation was required. In Fig. 8 the active TPBs are displayed for the case when another multifunctional material, a mixed electronic–ionic conductor (MEIC) is included in the electrode composition. It is apparent that not all multifunctional materials have an equivalent effect on the formation of active TPBs, as the active TPB counts are similar, but not equivalent. The optimal composition for the two cases actually happens to be approximately the same, but the peak number
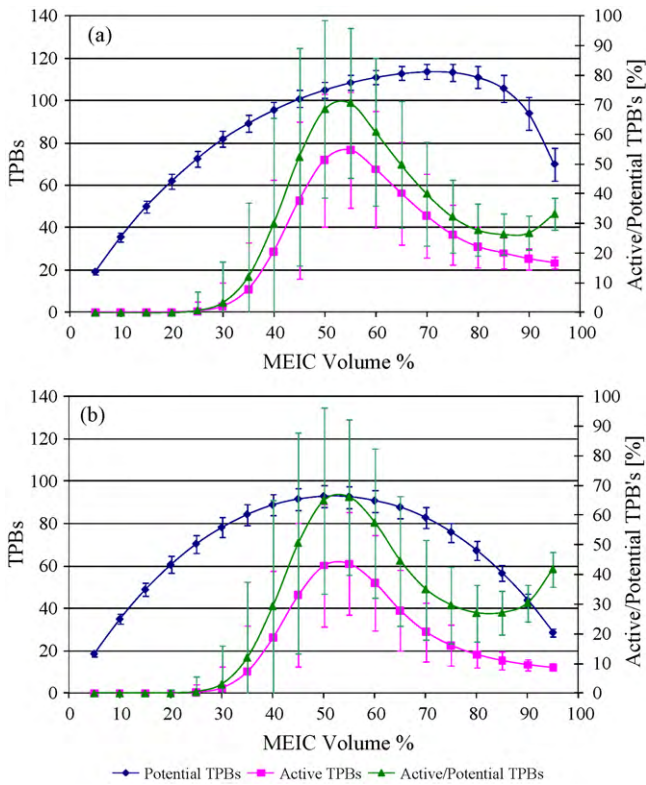


**Fig. 7.** Sample conductivity ($\kappa/\kappa_e$) and polarization resistance ($R_p$) calculation for randomized electrode (data from Sunde [16]).

**Fig. 8.** TPB counts for an all MEIC electrode (a) with and (b) without the physics of surface exchange and transport phenomena.

of active TPBs is not equivalent, with slightly more TPBs generated in a structure composed of MEIC materials rather than separate, highly porous electronic and ionic conductor phases. In addition, there is a marked asymmetry in the dependence of active TPBs on composition for the case with the MEIC, due to gas-phase percolation limitations and a noted competition between electronic and gas-phase percolation. However, in the model with highly porous electronic and ionic phases, this limit is completely removed due to the presence of gas phase in the entire electrode. Without these gas phase limitations in the model, and with the chosen boundary condition, the electronic and ionic phase percolation characteristics are equivalent. Thus, a symmetric active TPB dependence upon composition is expected with these assumptions, although these assumptions neglect important gas-phase percolation physics and boundary condition limitations extant in real fuel cell interfaces.

### 3.3. Gas-phase percolation effects on conductivity

Through the reconstruction of the interface model without gas phase limitations, the model's basic functions are verified and shown to provide similar predictions regarding the behavior of interfacial conductivity dependence on electrode composition. However, the electrode as modeled for this verification does not include the full capability of the model as formulated in the current work; for example, the effect of gas-phase percolation on conductivity has not yet been presented. To address this, the full model, with gas, electronic, and ionic phase percolation requirements, was run to garner insights into the effects of including more percolation physics on the interfacial conductivity dependence on electrode–electrolyte interface properties. In addition, the model was run both with and without accounting for the physics of surface exchange and transport phenomena. Figs. 9 and 10 present the conductivity results, as well as active TPB counts, for the cases without and with surface exchange and transport phenomena, respectively.
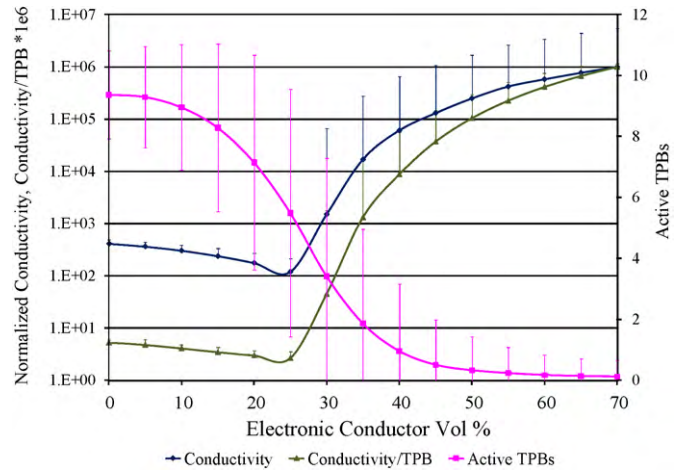


**Fig. 9.** Conductivity of composite electrodes without surface exchange and transport phenomena, accounting for gas-phase percolation.

It should be noted that, in general, the conductivity trends in these figures are similar to those observed in the two models compared above. It should further be noted that this similarity is present in spite of the vastly different trends in the active TPB counts. However, there are slight differences in the conductivity trends that may be attributed to the differences in percolation effects. First of all, the conductivity results of Sunde always increase with increasing electronic volume fraction, even though the rate of increase changes. In contrast, the current model results predict that conductivity actually decreases with increasing electronic volume fraction until the composition reaches the critical value at which the sudden and rapid change in slope occurs. This may be attributed to the decrease in TPB counts over this range of electronic volume fractions; however, the overall trend is obviously not governed by the TPB counts alone. In the model without gas phase limitations, the decrease in slope of the conductivity trend is roughly correlated to the decrease in TPB counts, but the current model predicts that TPB counts almost always decrease. In the region of low electronic conductor, the conducting paths could be expected to be mostly ionic, but with significantly increasing proportion of electronic conductor as the composition is moved towards the all-electronic case. The conductivity of the ionic conductor is much lower than the electronic conductor. Thus, for a certain set of compositions, the increase in number of TPBs is offset by the relative length of the ionically conducting paths and their lower conductivity compared
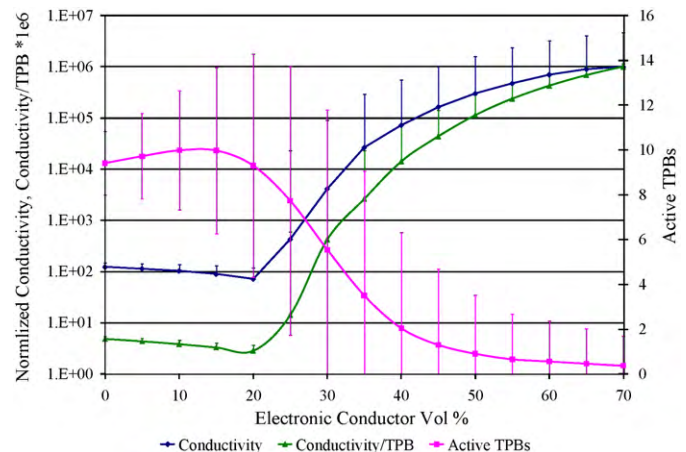


**Fig. 10.** Conductivity of composite electrodes with surface exchange and transport phenomena, accounting for gas-phase percolation.
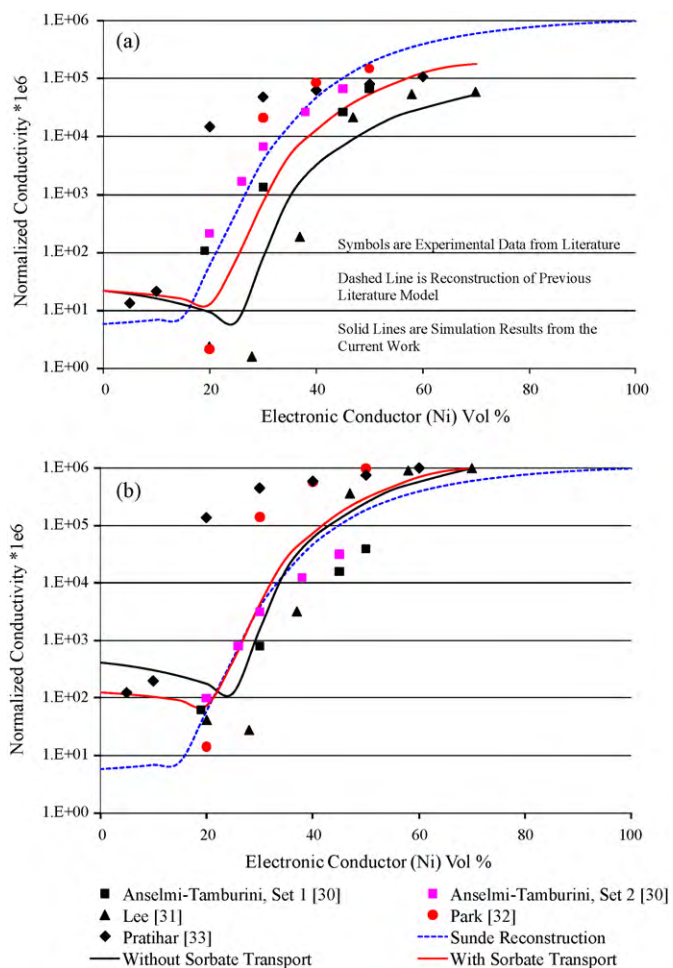
**Fig. 11.** Experimental data (symbols), previous model reconstruction (dashed line), and modeled results (solid lines) for conductivities of a Ni/YSZ electrode, normalized to (a) maximum in original Sunde results and (b) maximum within each set of results.

to electronically conducting paths. Clearly these results are related to the high phase contrast of the Ni–YSZ materials set. Nonetheless, at a certain composition (20–25% electronic conductor, as shown in Figs. 9 and 10), the effect of the higher conductivity of the electronic phase dominates over the effect of active TPB loss. Additionally, note that the inclusion of the gas-phase percolation shifted the sudden rise in conductivity closer to the previous model's prediction. It should also be noted that the effect of surface exchange and transport phenomena is only discernable in the calculated conductivities for electronic volume fractions above 20%. This limited range of effectiveness matches well with the limited range of effectiveness of surface exchange and transport phenomena in raising TPB counts, as shown in [21].

Although the current model's accuracy in predicting conductivity values has been verified through comparison to previous models, it is useful to understand how well each of these models predicts experimental observations with similar parameters and manufacturing methods that are closely approximated by the assumptions in each of the respective models. Comparisons of each model to experimental data are presented using two different normalization methods in Fig. 11, where symbols are experimental data found in literature, the dashed line is the reconstruction of Sunde's work from Fig. 6, and the solid lines present simulation results obtained with the current work's model. In part a, all data is normalized to the maximum conductivity presented in [20], thereby presenting a direct comparison of calculated and exper-

imentally observed conductivities. In part b, all data are internally normalized to their individual trend maximum values, thereby providing an improved understanding of how the trends internally compare. All data from previous experiments are presented with author permission. Conductivities predicted by each of the models and the various experimental data sets are all within reasonable agreement for almost all compositions, and all data trends are of roughly the same order of magnitude. In addition, the overall trends in the conductivity dependence on composition are similar; namely, conductivity remains relatively constant at low electronic conductor volume fractions, there is a sudden and dramatic rise in conductivity at some critical composition, and the conductivity approaches a plateau at high electronic volume fractions. Of particular importance is that the trends from all of the models investigated in this work lie within the spread of the experimental data over the range of compositions for which data was available. It should also be noted that under internal normalization, all three models predict similar values in the region of strong dependence on composition.

Although these trends are all generally similar, there are also discernable differences in key features of the experimental data and model results. In general, the experimental data appear to have sharper transitions in curvature than any of the model results. In addition, the experimental data exhibits a flatter plateau at high nickel content than the current model predicts, although the reconstructed model with the microporous material assumption captures this feature well. On the other hand, the actual values of experimental conductivity at these compositions better match the current model results. Without consideration of gas-phase percolation, the model seems to overpredict the conductivity by up to an order of magnitude in this region. It is worth noting that the original Sunde model may predict a different conductivity value than that presented here; however, the values of conductivity in the current reconstruction are expected to be similar because the underlying percolation properties were matched. Moreover, the lowest internally normalized conductivities of the experimental data are more closely predicted by the current model, and therefore the range of normalized conductivities and the ratio of the extreme values more closely predicted by the current model in any case. The experimental and modeled conductivity trends also display a substantial variation in the composition at which the sudden increase in conductivity with increasing nickel content begins. It is interesting to note that the highest and lowest nickel contents corresponding to this feature (30% and 5%, respectively), are exhibited by experimental data sets, with the modeled results lying within a range fairly in the middle of these values, and in good agreement with the other experimental data. The closest overall agreements between model and empirical data sets exist between the current model and the data of Lee et al. [31] and between the reconstructed model without gas-phase percolation and the data of Pratihar et al. [33].

Of particular interest is the behavior of conductivity at low nickel content. It can be seen that there are three trends exhibited by the data: relatively constant conductivity, mildly increasing conductivity with increasing nickel content, and decreasing conductivity with increasing nickel content. The model without gas-phase percolation seems to follow the first of these, while the current model follows the third trend. The original Sunde results followed the second of these trends. For much of the experimental data, behavior at very low electronic conductor volume fraction was unfortunately not collected; however, all three of these trends appear to be exhibited in the existing experimental data. The closest matches between model and experimental data again exist between the model without gas phase limitations and the Pratihar et al. [33] data and between the current model and the Lee et al. [31] data.

The relative matching between these particular pairs of data sets and models may be explained by the differences in the experimen-

tal methods and the expression of these features in the respective models. In the Pratihar et al. work the electronic conductor was incorporated by an "electroless" dip coating method onto YSZ powder [33]. On the other hand, the Lee et al. methodology followed more traditional powder processing techniques with large amounts of random mixing of powders of different phases [31]. The Pratihar et al. method carries with it the potential to impose a geometrical link between the electronic and ionic phases, possibly to increase the likelihood of TPB formation. The result of this may mimic the improved TPB formation exhibited by the model assumptions involved with the Sunde reconstruction, especially if the nickel-coated YSZ is sufficiently porous. However, the premise of this model and the Sunde model is the manufacturing of the electrode by random mixing, without any such geometric connection, which more closely matches the methods of Lee et al. Therefore, it is surmisable that the difference in the models at low electronic conductor volume fractions, for which TPB formation has been noted to compete equivalently with the effect of phase contrast, is due to this difference in electrode manufacturing processes. At higher nickel contents, the conductivity phase contrast effects are greater, and so the models and experiments more closely match in this regime.

## 4. Summary and conclusions

The Monte Carlo model presented in [21] has been extended to include the capability to investigate the role of electrode composition in overall conductivity of a composite SOFC electrode–electrolyte interface. Novel features of the model include gas-phase percolation, surface exchange and transport phenomena physics, the modeling of conduction pathways along particle boundaries, and the omission of charge-transfer and activation resistances. Model results are compared to those of a previous model and to various experimental results available in the literature. The assumptions of the previously reported conductivity model are incorporated into the current model to serve as a validation method for the current formulation.

This validation process showed that the current conductivity calculation algorithm is accurate while comparison to results of the previous model suggested the current model is useful for interfacial conductivity modeling. In particular, modeling conducting pathways along particle boundaries and excluding activation resistance were shown to result in conductivity trends that are not significantly altered from results previously reported. This allowed the current model to be used in a Monte Carlo method with sufficient iterations (10,000) to gather meaningful statistics.

Gas-phase percolation and surface exchange and transport phenomena physics were found to significantly alter the behavior of conductivity trends with respect to electrode composition. Competition between the percolation behavior and the effects of phase contrast led to separate regions of electrode composition where one or the other of these two factors dominates the conductivity trends. Models that include gas percolation and surface exchange and transport phenomena physics can more accurately model composite electrodes manufactured by certain methods. In particular, for Ni–YSZ electrodes manufactured by traditional powder process-

ing techniques, the current model that includes these phenomena more closely matches the behavior of the empirical data available, especially in electrodes with either very high ($\geq 50\%$) or very low ($\leq 15\%$) electronic conductor volume fraction.

## Acknowledgements

## References

[1] F. Tietz, H.-P. Buchkremer, D. Stover, Solid State Ionics 152/153 (2002) 373–381.
[2] S.B. Savignat, M. Chiron, C. Barthet, Journal of the European Ceramic Society 27 (2007) 673–678.
[3] C.-J. Li, C.-X. Li, M. Wang, Surface & Coatings Technology 198 (2005) 278–282.
[4] X. Ge, X. Huang, Y. Zhang, Z. Lu, J. Xu, K. Chen, D. Dong, Z. Liu, J. Miao, W. Su, Journal of Power Sources 159 (2006) 1048–1050.
[5] R. Zheng, X.M. Zhou, S.R. Wang, T.-L. Wen, C.X. Ding, Journal of Power Sources 140 (2004) 217–225.
[6] V.E.J. van Dieten, J. Schoonman, Solid State Ionics 57 (1991) 141–145.
[7] H.B. Wang, H.Z. Song, C.R. Xia, D.K. Peng, G.Y. Meng, Materials Research Bulletin 35 (2000) 2363–2370.
[8] G. Meng, H. Song, Q. Dong, D. Peng, Solid State Ionics 175 (2004) 29–34.
[9] K. Sasaki, J.P. Wurth, R. Gschwend, M. Godickemeier, L.J. Gauckler, Journal of the Electrochemical Society 143 (1996) 530–543.
[10] F.H. van Heuveln, F.P.F. Vanberkel, I.P.P. Huijsmans, Proceedings of the 14th Riso International Symposium on Material Science, 1993, p. 53.
[11] M.J.L. Ostergard, C. Clausen, C. Bagger, M. Mogensen, Electrochimica Acta 40 (1995) 1971–1981.
[12] M. Juhl, S. Primdahl, C. Manon, M. Mogensen, Journal of Power Sources 61 (1996) 173–181.
[13] V. Dusastre, J.A. Kilner, Solid State Ionics 126 (1999) 163–174.
[14] J.R. Wilson, W. Kobsiriphat, R. Mendoza, H.-Y. Chen, J.M. Miller, D.J. Miller, K. Thornton, P.W. Voorhees, S.B. Adler, S.A. Barnett, Nature Materials (2006) 541–544.
[15] P. Costamagna, P. Costa, V. Antonucci, Electrochimica Acta 43 (1998) 375–394.
[16] S. Sunde, Journal of the Electrochemical Society 143 (1996) 1930–1939.
[17] J. Deseure, Y. Bultel, L. Dessemond, E. Siebert, Electrochimica Acta 50 (2005) 2037–2046.
[18] A.V. Virkar, J. Chen, C.W. Tanner, J.-W. Kim, Solid State Ionics 131 (2000) 189–198.
[19] L.C.R. Schneider, C.L. Martin, Y. Bultel, L. Dessemond, D. Bouvard, Electrochimica Acta 52 (2007) 3190–3198.
[20] S. Sunde, Journal of the Electrochemical Society 142 (1995) L50–L52.
[21] A.S. Martinez, J. Brouwer, Electrochimica Acta 53 (2008) 3597–3609.
[22] S.B. Adler, Chemical Reviews 104 (2004) 4791–4843.
[23] A.S. Martinez, J. Brouwer, ASME Paper FuelCell2009-85191, June 2009.
[24] S. Torquato, Random Heterogeneous Materials, Springer, New York, 2002.
[25] D.J. Frank, C.J. Lobb, Physical Review B 37 (1988) 302–307.
[26] R. Fogelholm, Journal of Physics C 13 (1980) L571–574.
[27] R. Fogelholm, An Elimination Method for the Conductance of Percolation Networks, Royal Institute of Technology, Stockholm, 1980.
[28] R. Fogelholm, Proceedings of the 1981 ACM Symposium on Symbolic and Algebraic Computation, 1981.
[29] D.B. Gingold, C.J. Lobb, Physical Review B 42 (1990) 8220–8224.
[30] U. Anselmi-Tamburini, G. Chiodelli, M. Arimondi, F. Maglia, G. Spinolo, Z.A. Munir, Solid State Ionics 110 (1998) 35–43.
[31] J.-H. Lee, H. Moon, H.-W. Lee, J. Kim, J.-D. Kim, K.-H. Yoon, Solid State Ionics 148 (2002) 15–26.
[32] J.Y. Park, J.-H. Lee, J. Kim, H.-W. Lee, Key Engineering Materials 317/318 (2006) 905–908.
[33] S.K. Pratihar, A. Das Sharma, R.N. Basu, H.S. Maiti, Journal of Power Sources 129 (2004) 138–142.